



On the Reversion and Recrystallization of Austenite in the Interstitially Alloyed Ni-Free Nano/Ultrafine Grained Austenitic Stainless Steels

D. Rasouli¹ · A. Kermanpur¹ · E. Ghassemali² · A. Najafzadeh¹

Received: 11 October 2018 / Accepted: 27 January 2019 / Published online: 9 February 2019
© The Korean Institute of Metals and Materials 2019

Abstract

The martensite reversion treatment was conducted on two grades of Ni-free austenitic stainless steels interstitially alloyed with C and N. The hot rolled sheets of steels were cold rolled up to 80% thickness reduction to acquire strain-induced α' -martensite and subsequently reversion annealed at temperatures from 700 to 850 °C for 1 to 1000 s to revert the α' -martensite to austenite. Microstructural evolution was investigated using optical microscopy, X-ray diffraction, electron backscatter diffraction, and magnetic measurement techniques. Mechanical properties were measured using tensile tests at room temperature. The resultant microstructures contained both reverted and recrystallized austenite when reverted at 700 and 750 °C with the annealing time less than 100 s. A nonuniform grain structure was characterized under these conditions consisting of nano/ultrafine grains formed via α' -martensite reversion and coarser grains by recrystallization of the retained austenite. However, a more uniform austenite grain size with average size of 1 μm was obtained at 850 °C for 1000 s. The specimens having nonuniform grain structure exhibited excellent combinations of strength and ductility. A variety of mechanical properties was achieved depending on the annealing condition. The work hardening behavior affected UTS and ductility of the studied steels. The shift of the work hardening peaks to the higher strains was found suitable for ductility. Addition of C to N-containing Ni-free steels deteriorated mechanical properties. Best combination of strength and elongation was obtained in the test material with lower C/N ratio.

Keywords Interstitially alloyed austenitic stainless steel · Ni-free stainless steel · Reversion annealing · Recrystallization · Mechanical properties · Nano/ultrafine grain size

1 Introduction

Austenitic stainless steels (ASSs) are frequently used in various applications because of their easy processing, good mechanical properties, suitable corrosion resistance and adequate biocompatibility [1–3]. However, the yield strength of ASSs is normally low ranging from 350 to 450 MPa. To reduce weight for wide range of applications, there is significant interest to achieve combination of high strength-high ductility. Among different strengthening mechanisms, grain refinement is an interesting approach for improving strength

of engineering materials without significant loss in ductility. An innovative technique to acquire nano/ultrafine grain structure in metastable ASSs has been developed by several authors in which reversion annealing of the strain-induced α' -martensite (SIM) is controlled [4–6]. Based on chemical composition, the SIM fraction is increased with deformation and reaches a certain saturation level or complete transformation. Upon reversion annealing, the SIM reverts back to nano/ultrafine grained austenite under specific conditions via a shear or diffusional reversion mechanism [4–7]. The martensite reversion treatment has been used for grain refinement of some experimentally-produced and commercial Fe–Cr–Ni ASSs such as 301 [8, 9], 301LN [10, 11], 304 [12] 304L [13] and 316L [14] grades. Later, due to the high cost of Ni and its allergenic effect, the martensite reversion process was developed on Fe–Cr–Mn–low Ni ASSs such as 201 [15, 16], 201L [17] and recently on Ni-free Fe–Cr–Mn–N ASS [7].

✉ A. Kermanpur
ahmad_k@cc.iut.ac.ir

¹ Department of Materials Engineering, Isfahan University of Technology, Isfahan 84156-83111, Iran

² Department of Materials and Manufacturing, School of Engineering, Jönköping University, P.O. Box 1026, 551 11 Jönköping, Sweden

Due to the high cost of Ni and to the anticipated possibility of its allergic effect in human body, Ni-free, N-bearing ASSs with more suitable combination of strength, toughness and corrosion resistance are considered to be a good alternative for the traditional Cr–Ni stainless steels [18]. N is known as an efficient austenite stabilizer [19–21]. It is reported that the interstitial N has a great solid solution strengthening ability which consequently leads to an increase in the strength of stainless steels without affecting their good ductility and toughness as long as the solubility limit of N in austenitic is not passed [19, 22, 23]. Although N enhances strength and ductility of these steels, it deteriorates toughness at low temperatures [24]. N also has low solubility in molten iron and increases production challenges by utilizing the high pressure metallurgy [25]. In the past years, a new alloying system has been introduced in which C is used as the austenite stabilizer in association with N to obtain excellent properties in economic way [26]. Fe–Cr–Mn–C–N stainless steels alloyed by C+N, have been investigated by several authors [27–31]. As a result, a higher strength, ductility, impact toughness, fatigue life, and improved wet corrosion resistance are achieved in these new stainless steels [26, 27, 32]. The synergetic influence of C+N alloying has been introduced as responsible to improved properties [32]. The replacement of Ni by Mn increases the interstitial solubility of C and N [33]. Simultaneous alloying by C and N, increases the solubility of N and reduces the production difficulties [34].

It is evident that addition of C+N has strong effect on crystal lattice parameter of austenite. Among the alloying elements, C and N have the most effect on yield strength [35]. In many previous studies, the C and N content up to 1 wt% has been used to influence strength, but this amount of C+N retards SIM transformation. The effect of C+N at amounts greater than 0.5 wt% on ASSs has been investigated by several authors [27–32] but there are a few studies at low level of C+N (below 0.5 wt%) [36–38]. In addition, there is a limited investigation on the influence of C/N ratio on mechanical properties of the developed steels. In this work, microstructure and mechanical properties of the metastable ASSs containing different amount of C/N are investigated and the effects of martensite reversion thermomechanical treatment on microstructure, deformation mechanism, mechanical properties and work hardening behavior is studied. Microstructural evolutions during the martensite reversion treatment were conducted to investigate the underlying mechanisms contributing to the mechanical properties.

2 Material and Experimental Procedures

2.1 Casting of the Steels

The steel samples used in the current study were prepared in a 10 kg vacuum induction melting furnace under N partial pressure. Initially, the feedstock was melted under an argon atmosphere with partial pressure of 300 mbar. In order to introduce N into the molten steel, N gas stream with the partial pressure of 150 and 250 mbar was fed to the furnace for casting the C13–N17 and C06–N27 samples, respectively. The chemical composition of the as-cast steel samples is given in Table 1. The chemical composition of the alloy was determined by optical emission spectroscopy (OES). The concentration of C and N was measured by combustion analysis with the uncertainty of 0.003 and 0.001 wt%, respectively.

2.2 Thermomechanical Treatment

Precipitation of carbides and nitrides in ASSs deteriorates mechanical and corrosion properties. The most common precipitate in ASSs is $M_{23}C_6$ and in high N ASSs is M_2N that precipitate at grain boundaries [39, 40]. Therefore, the solution annealing and deformation temperatures should be selected appropriately to prevent from precipitation of the nitrides and carbides. To investigate the austenite stability and selection of suitable annealing and deformation temperature, thermodynamic calculations were conducted using the Thermo-Calc software with the TCFE7 steels database in temperature range of 673–1873 K (400–1600°C). Figure 1 shows vertical section of phase diagrams as a function of C wt% by varying N. It can be seen that by increasing C+N, austenite stability region expands. Also by increasing C content, the stability limit of $M_{23}C_6$ was shifted to higher temperatures. Same trends can be seen in precipitation temperature of M_2N nitrides by increasing N content.

The variation of phase fractions as a function of temperature was calculated as illustrated in Fig. 2. As seen, by increasing C/N ratio, the δ -ferrite phase fraction increases and temperature of formation shifts to lower temperatures because N is less prone to the formation of delta ferrite than C. Calculations also showed that increasing C/N ratio leads to increasing the volume fraction of carbides. In the C13–N17 steel this fraction is higher than M_2N volume fraction.

The as-cast ingots were cut into specimens of 30(width) × 15(thickness) × 70(length) mm ground blocks.

Table 1 Chemical composition of investigated steels (in wt%)

Alloy	Cr	Mn	C	N	Mo	Si	Fe	C+N	C/N
C06–N27	17.10	11.30	0.06	0.275	0.004	0.27	Bal.	0.33	0.22
C13–N17	17.60	12.00	0.13	0.170	0.003	0.32	Bal.	0.30	0.76

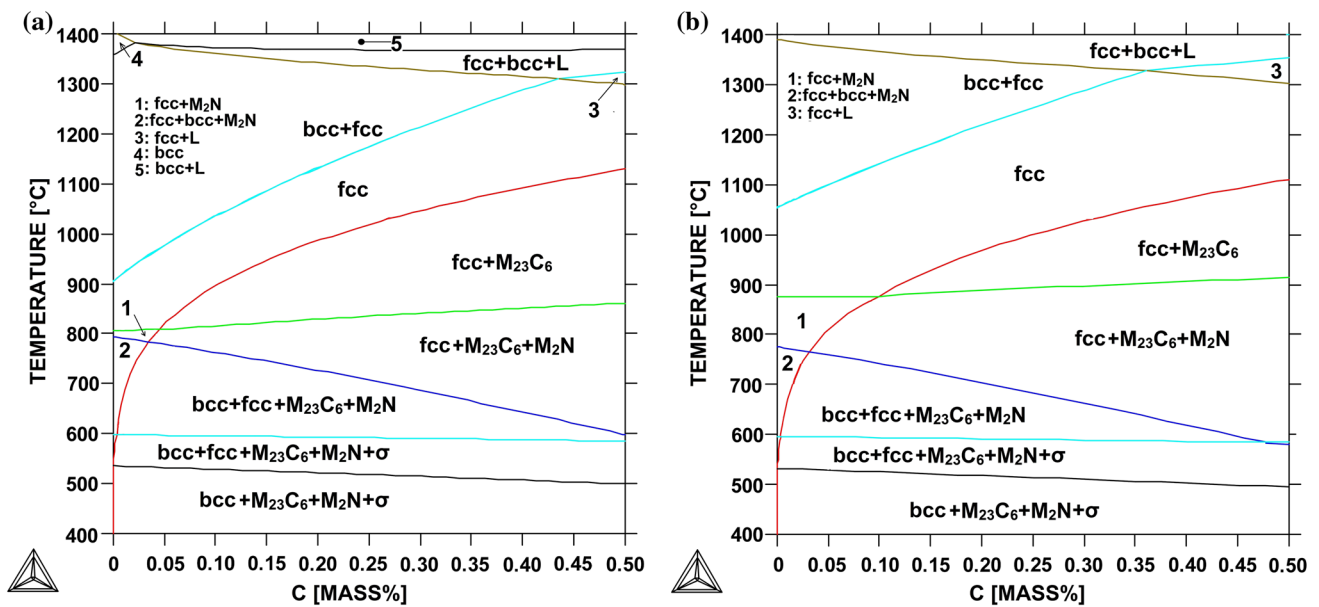


Fig. 1 Vertical section of calculated equilibrium phase diagrams by varying C content for Fe-18Cr-12Mn-C-N steels with: **a** N=0.15 wt%, **b** N=0.25 wt%

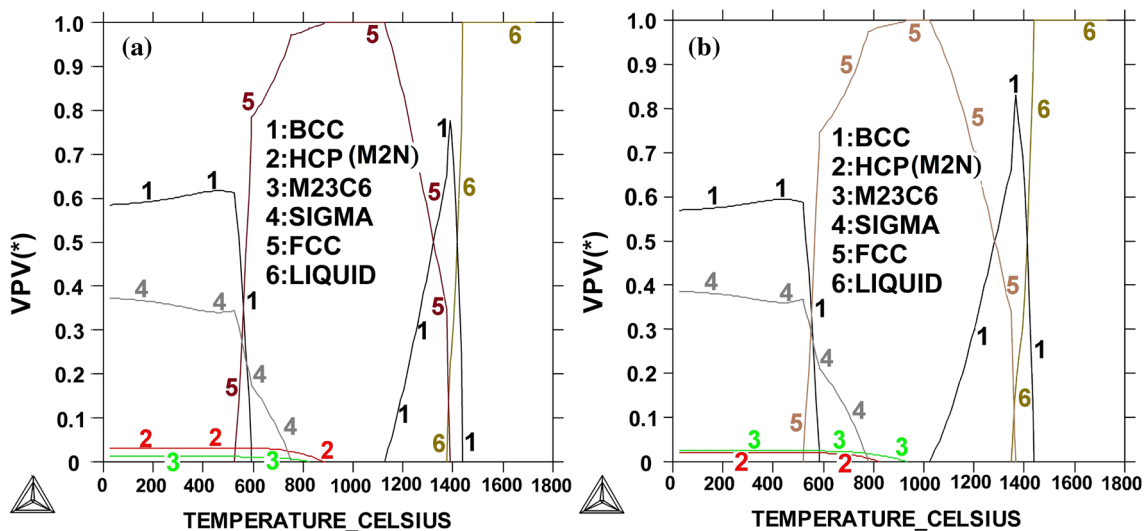


Fig. 2 Calculated molar fractions of the equilibrium phases in: **a** C06-N27, **b** C13-N17 steels

In order to dissolve carbides and carbo-nitrides and to lower segregation of elements occurring during solidification, the as-cast microstructure should be homogenized in the γ stability field. The heat treatment temperatures were selected to approach the upper stability limits of the γ single-phase field, calculated based on the respective C content. As depicted in Figs. 1 and 2, increasing C content shifted the stability limit of $M_{23}C_6$ ($Cr_{23}C_6$) to higher temperatures. Accordingly, C13-N17 and C06-N27 samples were homogenized at 1000 °C and 1100 °C for 8 h, respectively. The

samples were water quenched to avoid generation of precipitates during cooling.

The Thermo-Calc calculated results show that the only stable phase in both steels at temperature of 1000 °C is austenite and thermodynamically, the probability of precipitate formation is very low. Therefore, this temperature was chosen for hot rolling.

The formation of Cr_2N precipitates from kinetics point of view, was also investigated by relation suggested by Dai et al. [41]:

$$\begin{aligned} \ln t_s = & -9.9 + \frac{324.8}{1348 - T} + \frac{10723.7}{T} + \frac{89.0\text{Mn}}{T} \\ & + \frac{130.6\text{Cr}}{T} - \frac{171.5\text{Ni}}{T} \\ & - \frac{3241.7(1.2\text{N} + \text{C})}{T} + \frac{44.5\text{Mo}}{T} - \frac{3701.3\text{V}}{T} \end{aligned} \quad (1)$$

where t_s is incubation time period of Cr_2N precipitation in minutes and T is the temperature. Calculated t_s for samples are shown in Fig. 3. Also, the kinetics of M_{23}C_6 precipitation in Fe–Mn–Cr–C–N austenitic steels is studied by Roncery et al. [39]. Therefore, if deformation occurs at 1000 °C and above, kinetically, the formation time of precipitates is long enough for deformation of steels.

After homogenization, multi-pass hot rolling was conducted in a single-stand rolling mill at 1000 °C to reduce the specimens' thickness down to 6 mm. Following the rolling, specimens were water quenched to establish austenitic structure without any nitride and carbide precipitation. In order to eliminate contribution of the dislocation hardening to strength, samples were annealed at 1000 °C for 1 h followed by water quenching. To prepare samples for reversion annealing, multipass cold rolling up to 80% thickness reduction was performed with the strain rate of 0.5 s^{-1} and of 0.2 mm reduction in thickness per each pass. The reversion treatment of cold rolled samples was conducted by isothermal annealing temperatures of 700, 750, 800 and 850 °C for different times of 1–1000 s using a salt bath furnace.

2.3 Characterization Methods

Microstructures were characterized using X-ray diffraction (XRD; Phillips Expert MPD) at room temperature in angle range of 30–100° with $\text{Cu-K}\alpha$ radiation. The volume fraction

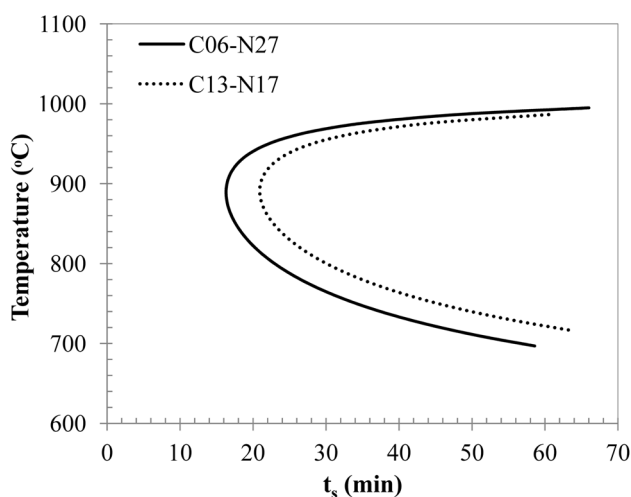


Fig. 3 Influence of temperature on the incubation period (t_s) of Cr_2N precipitation in designed steels calculated using Eq. (1)

of SIM was measured with a Feritscope (FMP30, Helmut Fischer GmbH). When measuring the α' -martensite content of the ASSs, the Feritscope readings were converted to the actual martensite contents using the following equation [42]:

$$\alpha' \text{-martensite content} = 1.71 \times \text{Feritscope reading} \quad (2)$$

Microstructural examinations were performed using optical microscopy (OM) (Nikon, LV100ND). Electron Backscatter Diffraction (EBSD) technique were used to quantify the microstructure and to access texture of the steel samples. In this analysis, firstly the specimen surfaces were polished with a diamond suspension down to 1 μm followed by chemical polishing using a 0.05 μm colloidal silica suspension. The EBSD information were acquired using the electron beam conditions of 15 kV accelerating voltage and 5 nA current in a scanning electron microscope (JEOL 7001F). The step size of 0.2 μm was selected for such analysis. The TEAM v4.4 and OIM Analysis™ v8 softwares were used for data collection and data analysis, respectively.

In the OM and XRD tests, the mechanically-polished specimens were first electrolytically polished in a solution consisting of 25 gr CrO_3 , 133 cc acetic acid and 7 cc water at temperature range of 17–19 °C and at an operating voltage of 20–22 V for 4–6 min. Several flat tensile specimens with 25 mm gauge length were machined from the sample sheets according to standard technique (ASTM: E8) along the rolling direction [43]. Tensile test was performed with an Instron-type tensile test machine at 25 °C with the strain rate of 0.001 s^{-1} . The strain was measured using a calibrated laser extensometer. Strain hardening rate (SHR) was numerically determined by using the SLOPE command in Excel software.

3 Results

3.1 Cold Rolled Structures

Figure 4 shows OM images of the raw materials after hot rolling and annealing. A recrystallized microstructure can be seen in both samples. The annealing twins were readily observed inside some grains, which is a characteristic feature of the alloys with low stacking fault energy (SFE). According to Feritscope readings, volume fraction of delta ferrite in Fig. 4a, b determined to be < 5% and 7%, respectively. It is seen that the raw materials have a recrystallized microstructure with the grain size of 56 ± 8 for C06–N27 and $49 \pm 9 \mu\text{m}$ for C13–N17 steels.

Figure 5 shows the evolution of SIM volume fraction of test materials during cold rolling. As it can be seen, the SIM content was increased and the rate of SIM transformation was decreased with increasing of thickness reduction.

Fig. 4 Microstructure of steels after hot rolling and annealing: **a** C06–N27, **b** C13–N17

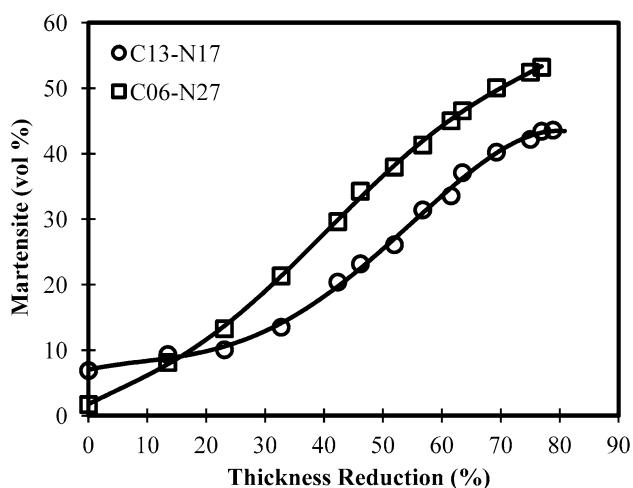
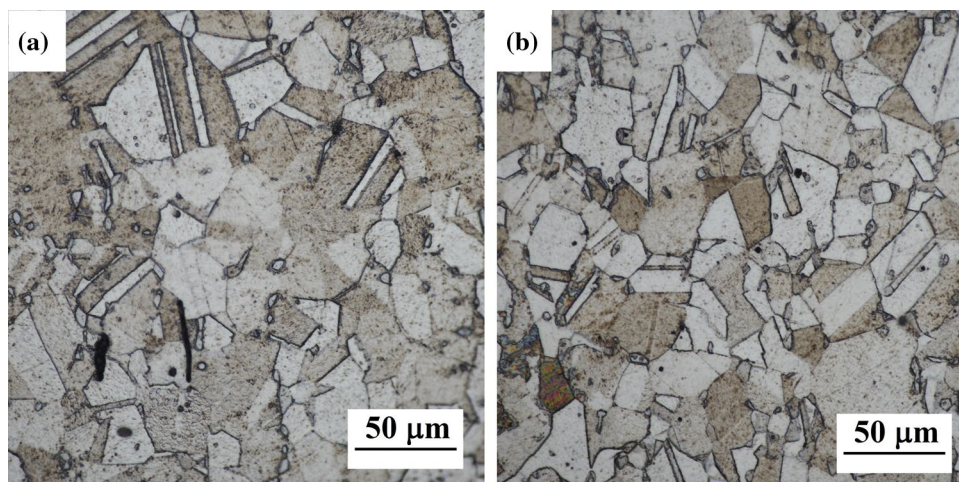


Fig. 5 Influence of cold rolling reduction on SIM volume fraction of test materials

Comparing these two curves, it can be observed that at a C + N content of 0.3 wt% approximately, more SIM is formed in the specimen with lower C/N ratio by thickness reduction of 80%. It seems that C suppressed the SIM transformation.

In a study by Masumura et al., a thermal and deformation-induced α' -martensite transformation behaviors between carbon- and nitrogen-added metastable austenitic stainless steels were investigated. They showed that carbon enhance the mechanical stability of austenite in comparison to nitrogen-added steel, in contradiction to the effect of carbon and nitrogen on thermal stability [44]. On the other hand, the stability of austenite is also dependent on the grain size. Noticing the Fig. 4, it can be seen that the austenite grain size in C06–N27 steel is bigger than C13–N17. It is expected that stability of austenite in C06–N27 steel be higher than C13–N17 Steel. Since the difference in average grain size (AGS) of steels is only about 7 μm , the effect of grain size

on austenite stability could be small. Although, it is shown that the thermal stability of austenite significantly depends on the grain size but the mechanical stability of austenite is independent of the grain size. [45].

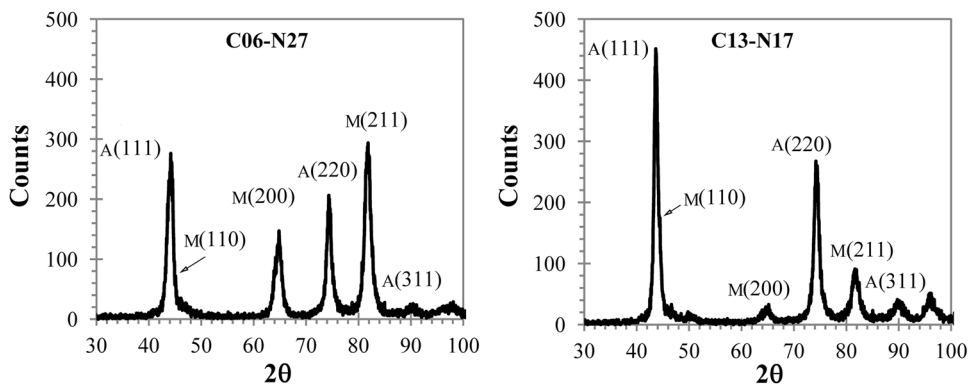
The XRD patterns of samples after cold rolling are shown in Fig. 6. It can be seen that in both samples the α' -martensite was formed. The amount of α' -martensite in C06–N27 sample is higher than C13–N17 samples, which is due to the lower stability of austenite with the smaller C/N. There is also no ϵ -martensite peak in the patterns which indicates that ϵ -martensite content in samples is lower than about 1%.

3.2 Microstructure Evolution During Reversion Annealing

It is shown that controlled annealing of SIM in ASSs could result in a sufficient reversion of α' -martensite to austenite [4]. This process depends on annealing time and temperature and SFE of the material. No ϵ -martensite was identified using XRD data after 80% cold rolling (Fig. 6). A source of. In any case, the ϵ -martensite, if present, during the heating or at the start of the annealing would revert very quickly [46]. Therefore, there is only α' -martensite during annealing stage and the mechanism and kinetics of its reversion is of importance.

Following cold rolling, the content of α' -martensite varied between the steels; therefore, for comparison, the quantity of reverted α' -martensite is considered as a percentage of the initial α' -martensite content of steel using the relative reverted fraction. Figure 7 shows the relative reverted percentage of steels at different annealing times and temperatures obtained by Feritscope measurements. The rate of martensite reversion is high with the onset of annealing (time of less than 10 s) and saturation is reached by further annealing. At the same annealing temperature, the reversion kinetics is similar in both steels and there is no significant

Fig. 6 XRD patterns of the cold rolled samples



difference between them. At 800 and 850 °C, more than 90% of α' -martensite was transformed back to austenite within 10 s.

It is accepted that at the initial stage of annealing, density of lattice defects such as dislocations acting as nucleation sites for the austenite reversion is high, resulting in a higher reversion rate. As the annealing continues, the defect density is intensely reduced, causing a lower reversion rate [5]. Rajasekhara et al. [10] suggested that during the initial periods of annealing, occurrence of extremely rapid grain growth is related to the high grain boundary curvature which results in a large driving force for the grain growth.

It can be seen in Fig. 7 that at low annealing temperature (700 °C), almost an austenitic microstructure can be obtained only by long time annealing (1000 s). Whereas, at high annealing temperature (850 °C), almost a fully austenitic microstructure was obtained even at short annealing times (10 s).

Microstructural evolution in steels for annealing at temperatures of 700 and 850 °C was investigated by means of EBSD (Figs. 8, 9). In both steels, after 10 s at 700 °C, the structure was entirely complex, comprising of α' -martensite, large-grained retained austenite, nano/ultrafine reverted austenite grains and δ -ferrite, as shown in Figs. 8a and 9a for the C06–N27 and C13–N17 steels, respectively. In both steels, after 100 s annealing at 700 °C most of α' -martensite was reverted (Figs. 8b, 9b) and after 1000 s recrystallization of

the retained austenite is completed and all α' -martensite was reverted to austenite (Figs. 8c, 9c). The resultant grain size distribution was nonuniform as shown in Fig. 10. It is well established that the bimodal microstructures provide enhanced strength–ductility synergy since large grains provide plastic strains while small grains support necessary strength [47].

By annealing at 850 °C, more than 90% of α' -martensite reverted to austenite within 10 s for both steels (Figs. 8d, 9d). Fast reversion is typical feature of the shear type reversion [4]. At 10 s, a complex microstructure consisting of large recrystallized retained austenite and nano/ultrafine grained reverted austenite can be seen (Fig. 8d). At 100 s, microstructure was the same but grain growth occurred for reverted austenite grains. At 1000 s, more uniform grain size distribution can be seen in both steels. Two mechanisms occurred at 850 °C: while (1) the austenite reversion was completed for 10 s, (2) the recrystallization of retained austenite progressed during the first 100 s, as shown in Figs. 8e and 9e (as examples, the arrows in Fig. 9d shows the new grains nucleated on retained austenite grain boundaries). These phenomena resulted in a bimodal grain size distribution in which large grains are formed from retained austenite and the ultrafine grains from the reverted α' -martensite. This is further indicated in the grain size distribution in steels annealed at 850 °C for 1000 s (Fig. 10). The frequency distribution changes between the investigated steels and grain

Fig. 7 The variation of relative reverted percentage as a function of annealing time at different temperatures for: **a** C06–N27 and **b** C13–N17 samples. The lines connecting the points are added for better presentation of results

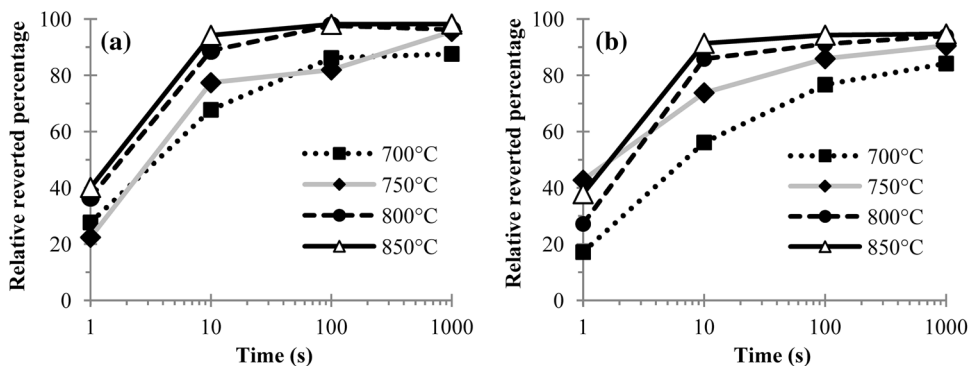
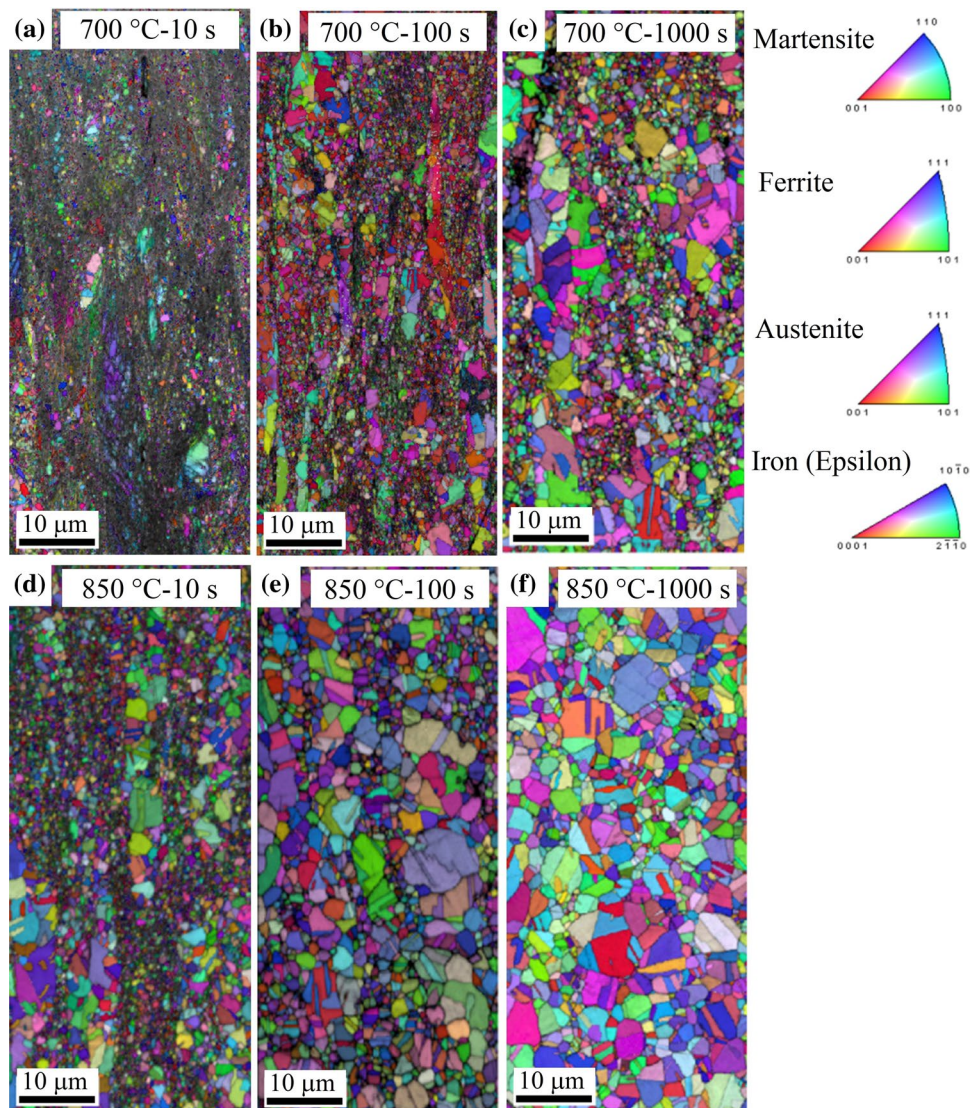


Fig. 8 a–f Inverse pole figure maps of the C06–N27 steel at different annealing conditions



types. For the reverted grains, the highest frequency was occurred at $0.207\ \mu\text{m}$ for C06–N27 and at $0.226\ \mu\text{m}$ for C13–N17 steels.

Comparing the microstructure of samples annealed at $700\ ^\circ\text{C}$ with those annealed at $850\ ^\circ\text{C}$, it can be concluded that higher annealing temperatures are more suitable for achieving a uniform grain size. As it is shown in Figs. 8f and 9f, after annealing at $850\ ^\circ\text{C}$ for 1000 s, the grain size became relatively uniform due to the growth of reverted grains.

The average grain size of samples is shown in Fig. 11. The smallest grain size was $191\ \text{nm}$ observed in C06–N27 steel annealed for 100 s at $700\ ^\circ\text{C}$. In C13–N17 steel, the smallest grain size was $210\ \text{nm}$, observed in the sample annealed for 100 s at $700\ ^\circ\text{C}$. One reason for the observed variation in grain size is related to the fact that the austenite nucleation is occurred through different mechanisms (diffusion or shear type) during the annealing process [16].

3.3 Mechanical Properties of Steels After Reversion Treatment

To study the influence of reversion treatment on mechanical properties of steels, tensile strength, elongation and strain hardening behavior of different reversion-treated specimens were determined. The yield strength, ultimate tensile strength (UTS) and fracture elongation of steels are shown in Fig. 12. It can be seen that the variation trend of mechanical properties at the same annealing time and temperatures were similar in both steel grades: the samples with lower annealing time and temperature mainly have high yield strength and UTS with low ductility. By increasing the annealing time and temperature, UTS is decreased and ductility is improved. Generally, the elongation of C13–N17 steel (with higher C/N ratio) is lower than C06N27 steel (with lower C/N ratio). Therefore, it seems that in comparison to alloying with N, at constant

Fig. 9 a-f Inverse pole figure maps of the C13–N17 steel at different annealing conditions

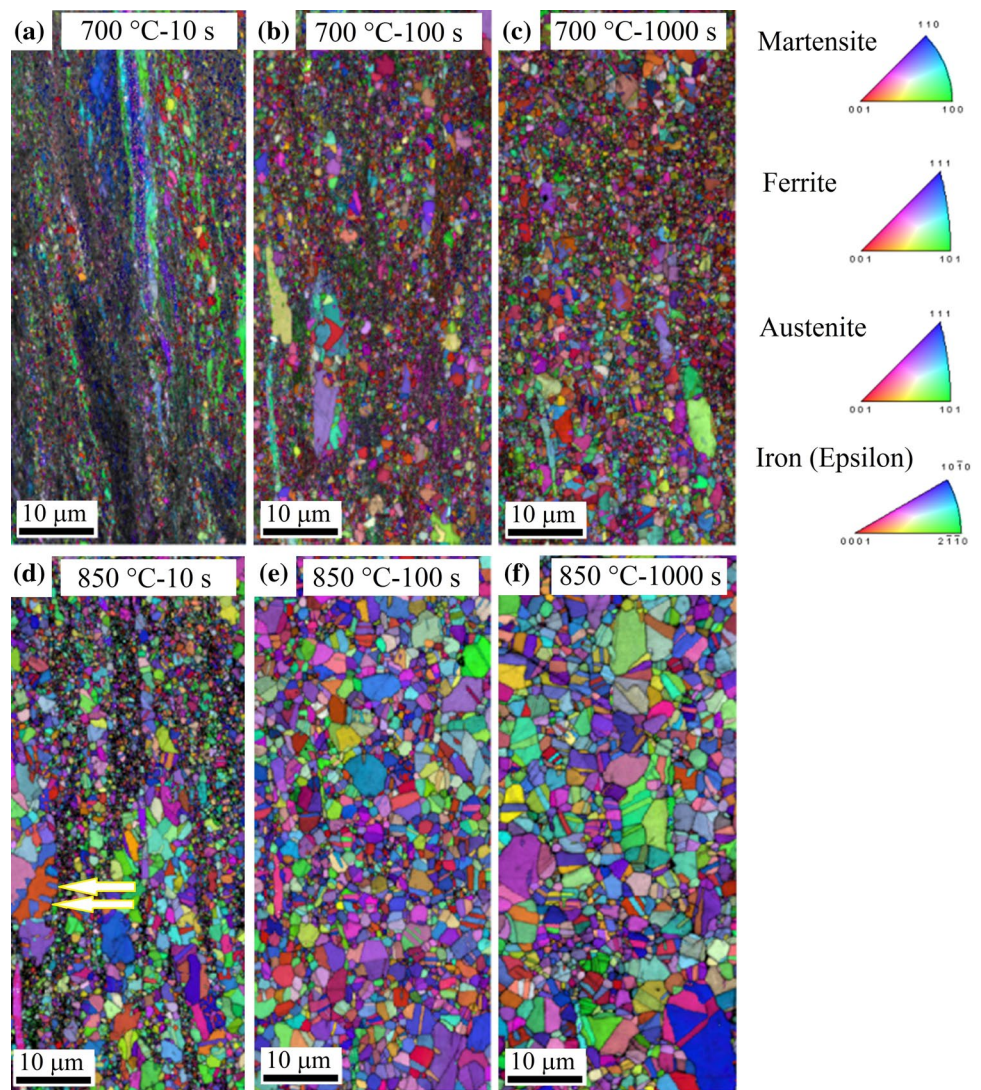
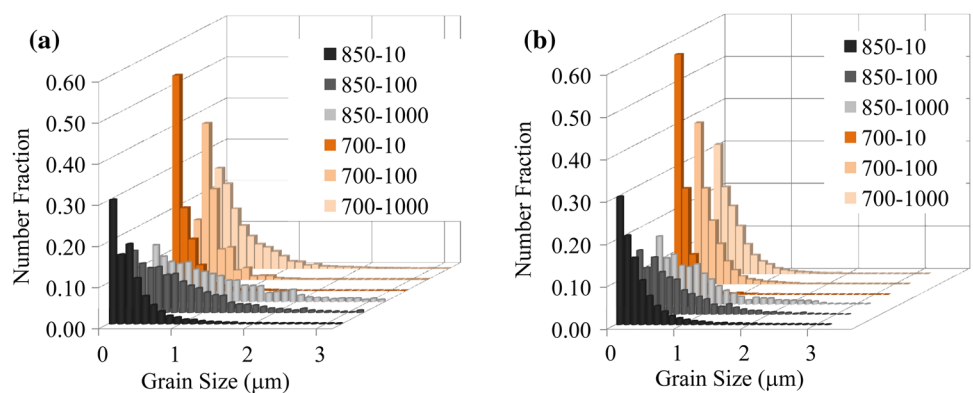


Fig. 10 Grain size distribution of C06–N27 steel (a) and C13–N17 steel (b) at different annealing conditions



level of interstitial alloying, C has detrimental effect on mechanical properties. N increases the concentration of free electrons, whereas carbon contributes its electrons to the more brittle covalent bonding [48]. The distribution

of nitrogen in binary fcc Fe–N alloys is characterized by short range atomic ordering, while no atomic order is revealed in the Fe–C austenite [48].

Fig. 11 Average grain size distribution of **a** C06–N27 and **b** C13–N17 specimens at different annealing conditions

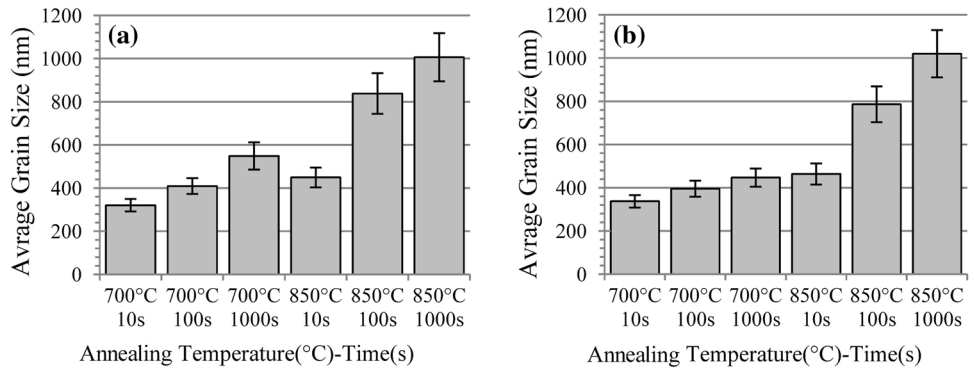
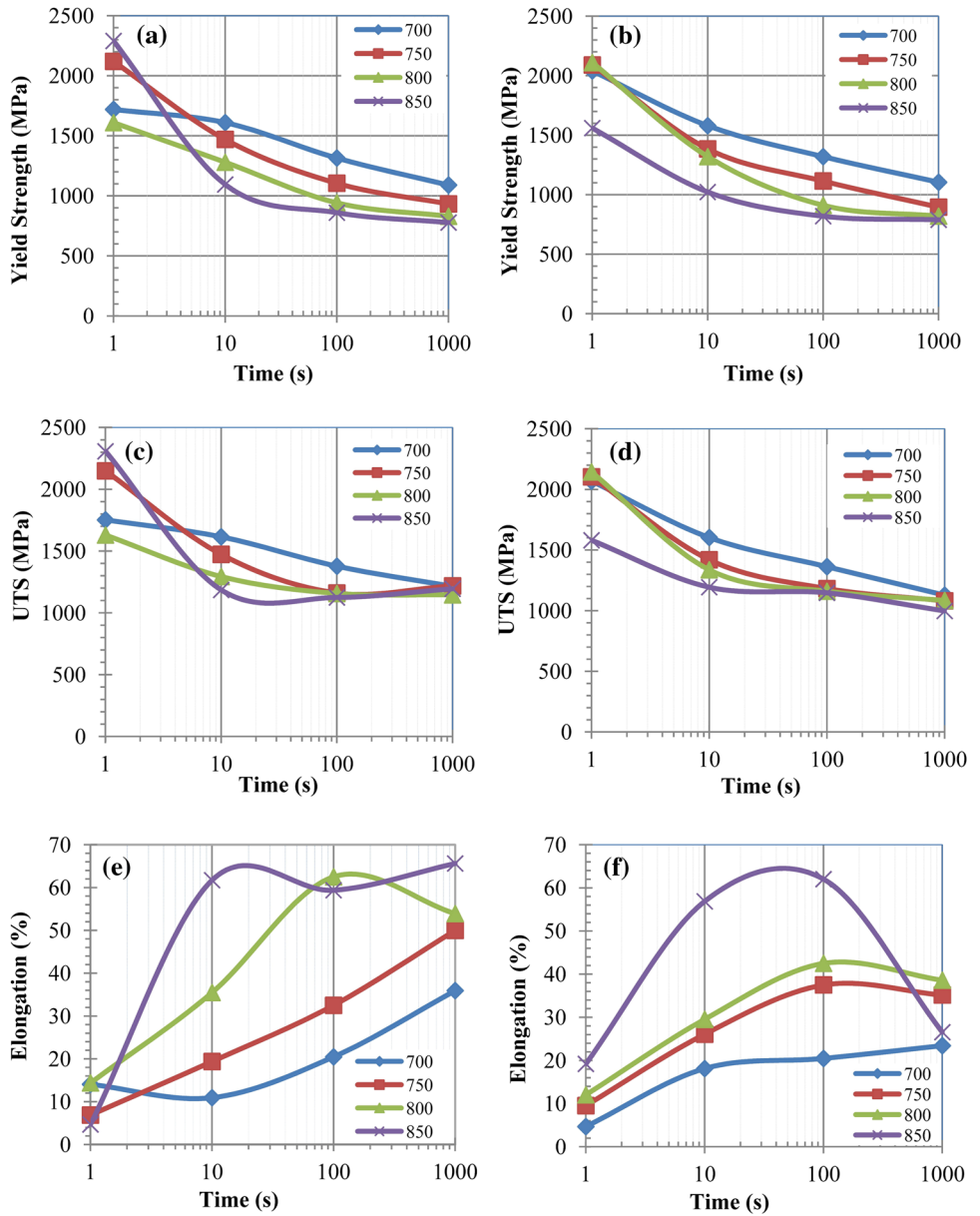


Fig. 12 Variation of yield strength, UTS and elongation of studied steels at different annealing conditions: **a, c, e** C06–N27 and **b, d, f** C13–N17

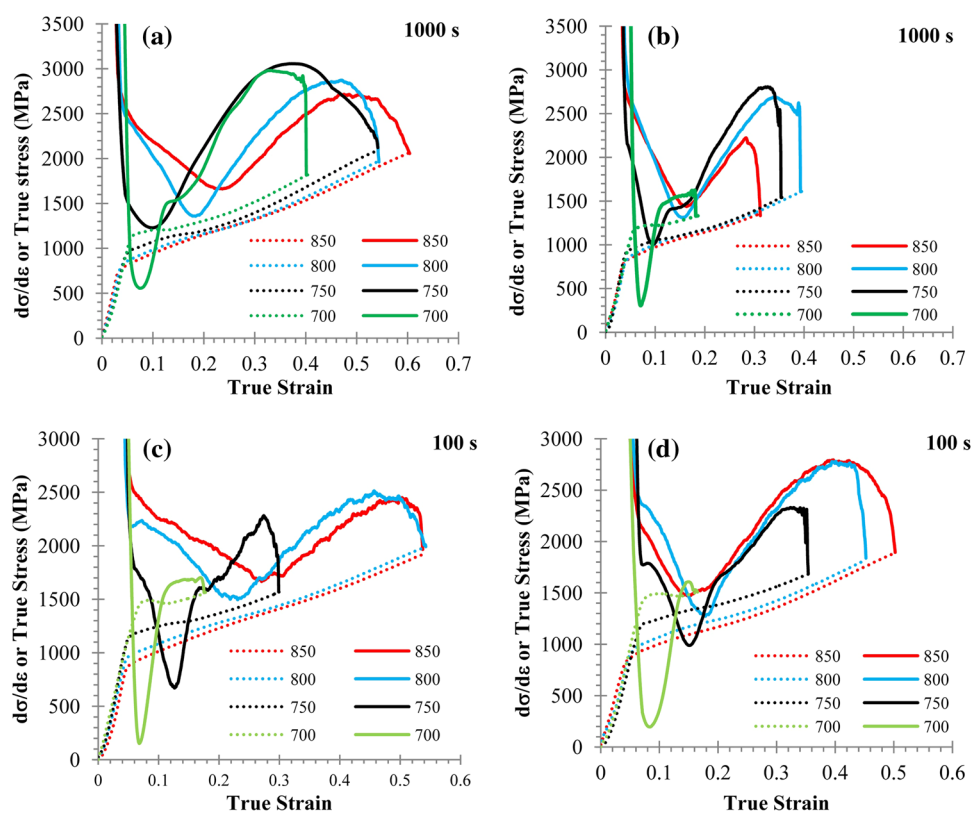


As depicted in Fig. 12, for the C13–N17 steel at determined annealing time and temperature, UTS was lowered by increasing annealing time. However, for the C06–N27 sample annealed at 850 °C, UTS firstly decreases then increases slightly. The variation of elongation in this sample was also different from the C13–N17 steel and by increasing the annealing time, elongation was increased. This can be related to low C content of this sample (lower C/N ratio). Based on Thermo-Calc calculations, by increasing the C content, volume fraction of $M_{23}C_6$ carbides was increased and volume fraction of M_2N precipitates was decreased. Therefore, in the C06–N27 sample the probability of M_2N precipitation was high. Kinetically, the formation of these precipitates at 850 °C required about 1100 s (Fig. 3) which is close to annealing time of the sample in the conducted experiments. Since the samples after annealing were water quenched, it is possible that very fine precipitates were formed in the microstructure, which resulted in an improved UTS and elongation compared to the C13–N17 sample. Behjati et al. [7] studied this matter on a steel with chemical composition of Fe–17.5Cr–11.5Mn–0.25N–0.05C (wt%) which has very close chemical composition to the C06–N27 steel in this study. They showed that nano precipitates sizing 30–40 nm are appeared in the samples annealed at 900 °C for 100 s. It was reported that the UTS is increased by the formation of these nano precipitates [7].

In both C06–N27 and C13–N17 steels, following annealing at 700 °C for 10 s (in which the microstructure consisted of α' -martensite, reverted and retained austenite), the yield strength was 1610 and 1580 MPa, while the uniform elongations were 11 and 18%, respectively. When annealing at 700 °C for 1000 s (in which the microstructure contained reverted and recovered, partially recrystallized austenite), the yield strength was declined notably in the C06–N27 steel to 1090 MPa and to 1105 MPa in the C13–N17 steel, while uniform elongations were 36 and 23%, respectively. The C/N fraction has little effect on the yield strength but large effect on elongation. More detailed tensile test data are given in Fig. 12. It might be noticed that yield strength of the grain refined steels are appreciably higher than that of conventional coarse grained steel (usually 350–400 MPa).

The true stress–true strain and the SHR curves of the steel specimens annealed at 700, 750, 800 and 850 °C are plotted in Fig. 13. The results show that in both steel specimens, for the steels annealed for 1000 s at 700 °C or higher up to 850 °C, a two-stage strain hardening behavior is exhibited, as already reported for metastable steels [5, 6, 49, 50]. At small strains, the SHR dropped strongly, approaching a minimum at a specific small strain, which depends on the reversion temperature. This strain implies to be the smallest strain for C06–N27 steel after annealing at 700 °C. In addition, the lowest SHR for the C13–N17 steel observed in sample annealed at 700 °C. At low annealing temperatures,

Fig. 13 True stress and strain hardening rate as a function of true strain for the **a, c** C06–N27 and **b, d** C13–N17 steels after annealing at different temperatures and times



the minimum SHR is lower than samples annealed at higher temperatures. The SHR attained a peak at a specific strain, which did not alter much between the specimens. At all instances, the SHR peak strain was increased by increasing the annealing temperature except for the C13–N17 steel annealed at 850 °C for 1000 s. For this steel, at 1000 s annealing, the SHR peak strain of 850 °C was lower than 750 and 800 °C. The UTS of this sample was lower compared to samples annealed at 750 and 800 °C.

4 Discussion

4.1 The Stability of Austenite

The stability of the investigated ASSs, alloyed with C+N, was so high such that the applied 80% cold reduction (entirely severe in practice), only resulted in a partial transformation to α' -martensite. Both steels had similar chemical composition and approximately same interstitial content. The only difference was the C/N ratio. In the C06–N27 steel with C/N=0.22 (lower C/N ratio), more transformation was observed compared to the C13–N17 steel with C/N=0.76. This can be discussed from SFE point of view. In fact, C increases the SFE of steel and suppresses the SIM transformation. The change in deformation microstructure according to SFE was reported by Lee et al. [30]. They explained change in deformation microstructure by larger increasing tendency of SFE via substitution of C for N and showed that there is a strong correlation among relative C fraction, SFE, and corresponding deformation microstructure. Compared with N, the relative increase in SFE by C addition, is larger, which is confirmed by the suppression of ϵ -martensite in the alloy with higher C fraction [30].

In a study by Reed and Schramm [51], it is estimated that C has significant effect on the SFE as following equation:

$$\text{SFE (mJ/m}^2\text{)} = 4 + 1.8\text{Ni} - 0.2\text{Cr} + 410\text{C (in wt\%)} \quad (3)$$

Equation (3) is valid for N content of 0.003–0.006 wt%, Cr content of 10–30 wt% and Ni content of 10–20 wt%. Brofman and Ansel [52] proposed a modified relation, using a four dimensional regression analysis on alloys with higher C content (up to 0.3 wt%):

$$\text{SFE (mJ/m}^2\text{)} = 16.7 + 2.1\text{Ni} - 0.9\text{Cr} + 26\text{C (in wt\%)} \quad (4)$$

Equation (4) is valid for N content of 0.003–0.05 wt%, Cr content of 10–20 wt% and Ni content of 10–20 wt%. Smaller coefficient of C at this equation indicates that an increment in 0.1 wt% C, increases the SFE only 2.6 mJ/m². Austin and Reed [53] reported that simultaneous addition of C+N to Fe–20Cr–10Ni steels, increases the austenite stability against the formation of SIM. They found that

C was more effective than N and relation is in the form of 3[C] + [N]. Although the SFE is not measured in their study, indirect observations showed an increase of SFE and retardation of ϵ -martensite formation by C. In a study by Lee et al. [30] on Fe–18Cr–10Mn–(0.39–0.69)N and Fe–18Cr–10Mn–0.4N–(0.15–0.42)C, the results of previous work were confirmed showing that addition of C increases the SFE and its effect is larger than N. They used a three-dimensional linear regression and proposed a relation as follows:

$$\text{SFE (mJ/m}^2\text{)} = -5.97 + 39.94(\text{C} + \text{N}) + 3.81(\text{C/N (in wt\%)}) \quad (5)$$

Equation (5) can be used up to N=0.7 wt%. In their study, ϵ -martensite formation and twinning was observed in the alloy with C/N=0.03. Whereas, in the alloy with higher C/N ratio, deformation twinning was reported as governing mechanism. Therefore, C has large tendency to increase the SFE and in alloys with higher C/N ratio, a lower SIM can be seen. The SFE of steels was calculated using Eq. (5) obtained by Lee et al. [30]. The calculated SFE for C06–N27 steel was 8 mJ/m² and for C13–N17 steel 9 mJ/m² showing negligible difference.

After cold rolling of steels, the retained austenite fraction was in the range of 40–50%. Hence, subsequent annealing would only partially refine grain structure through the martensite reversion, and recrystallization was needed for grain refinement of the deformed retained austenite. Although recrystallization depends on preceding deformation but its kinetics is smaller than the reversion, therefore a longer time and/or higher temperature for annealing is necessary to complete the recrystallization stage [5, 54]. Under this condition, grain growth could occur in the region of reverted nano/ultrafine grains during annealing. Consequently, a uniform refined grain structure can be achieved through a reasonable balance between the relative kinetics of the recrystallization and reversion mechanisms. Retardation of the reverted grain coarsening is possible through different mechanisms such as precipitation in grain boundary. Martins et al. [55] illustrated that the solid solution C, in comparison to the precipitated C, resulted in a material with a higher propensity to work hardening but less sensitivity to the formation of martensite. Precipitation of carbides and nitrides leads to bonding the C and N in precipitates, resulting in a reduction of the interstitial elements in solid solution. As a result, lower propensity to work hardening and higher sensitivity to the martensite formation can be expected.

4.2 The Effect of Reversion Annealing on Microstructural Evolution

During reversion annealing, the SIM is reverted back to austenite. The magnetic measurement studies have shown that the reversion process is very fast, especially at high temperature, where the main fraction of α' -martensite vanished

after 10 s at 850 °C (Fig. 7). The high reversion rate conveys that this process is a shear mechanism [4]. As shown in the EBSD data of Figs. 8a and 9a, areas with very fine grains and sub-grain boundaries were also detectable, representing a shear-reverted austenite with high dislocation density [4].

Somani et al. [5] approach can be used to evaluate the reversion mechanism of the alloys at annealing temperatures. They calculated the driving force of reversion ($\Delta G^{\alpha' \rightarrow \gamma}$) as a function of chemical composition and temperature based on Kaufman et al. [56] equation for ternary Fe–Cr–Ni alloys, as follows:

$$\begin{aligned} \Delta G^{\alpha' \rightarrow \gamma} (\text{J/mol}) = & 10^{-2} \Delta G_{\text{Fe}}^{\alpha' \rightarrow \gamma} (100 - \text{Cr} - \text{Ni}) - 97.5\text{Cr} \\ & + 2.02\text{Cr}^2 - 108.8\text{Ni} + 0.52\text{Ni}^2 \\ & - 0.05\text{NiCr} + 10^{-3}T(73.3\text{Cr} - 0.67\text{Cr}^2 \\ & + 50.2\text{Ni} - 0.84\text{Ni}^2 - 1.51\text{CrNi}) \end{aligned} \quad (6)$$

where T is the temperature in Kelvin, $\Delta G_{\text{Fe}}^{\alpha' \rightarrow \gamma}$ is the Gibbs free energy difference in pure iron, and the symbols of Ni and Cr represent the chemical composition of each element (wt%). As other alloying elements such as C, N, Mn, Mo, Si have also strong influence on driving force, their effects have been considered as using Ni_{eq} (Ni equivalent) and Cr_{eq} (Cr equivalent) instead of only Ni and Cr, respectively, in Eq. (6). Ni_{eq} and Cr_{eq} were determined for Fe–Cr–Ni system, using Eqs. (7) and (8) respectively, as follows:

$$\text{Ni}_{\text{eq}} = \text{Ni} + 0.6\text{Mn} + 20\text{C} + 4\text{N} - 0.4\text{Si} \quad (7)$$

$$\text{Cr}_{\text{eq}} = \text{Cr} + 4.5\text{Mo} \quad (8)$$

Using the Gibbs free energy of BCC and FCC structures, Tomimora et al. [4] reported that the driving force of at least 500 J/mol is needed for the shear mechanism regardless of the chemical composition of Cr–Ni alloys. Using Eqs. (6)–(8), the Gibbs free energy of steels was calculated (Fig. 14). As seen in Fig. 14, the predicted driving force for the both steels was higher than 500 J/mol at temperatures 700–1000 °C, conveying that the transformation should be of shear-type.

It is shown that with increasing heating rate above 10 °C/s the reversion mechanism changes from diffusional to shear-type [57, 58]. In the present work, the reversion treatment was conducted in a salt bath furnace, where the heating rate was above 10 °C/s, supporting the manifestation of the shear mechanism. However, fine and equiaxed austenite grains with random orientations, as the characteristics of diffusional reversion, have been also detectable in the microstructures, as shown in Figs. 8d and 9d. This shows that nucleation of new grains was a diffusion-controlled process. The results show that both types of martensite reversion are likely to occur at 700 °C. Although the α' -martensite vanishes after a few seconds at 700 °C and in 10 s at 850 °C, large retained austenite grains plus the

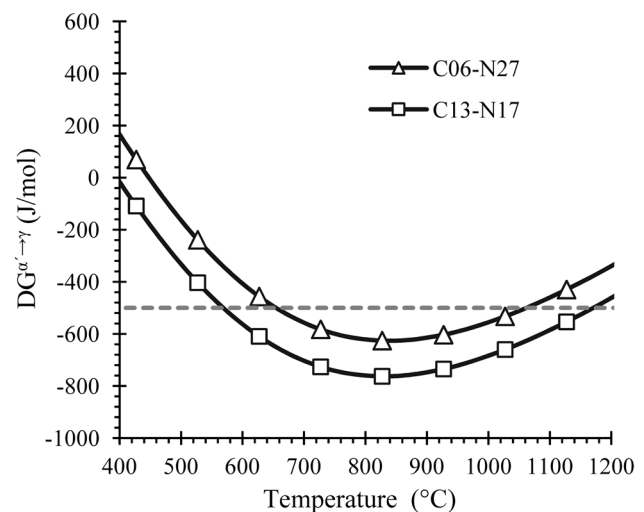


Fig. 14 Relation between temperature and Gibbs free energy changes from martensite to austenite in studied steels

shear-reverted austenitic regions were still awaiting for the commencement of recrystallization.

It is reported that recrystallization kinetics of the cold rolled and the shear-transformed austenite is lower than the reversion process taking place at the higher temperatures and longer times [54, 59]. This can be seen in Figs. 8 and 9 where conventional static discontinuous recrystallization of the retained austenite is completed at 850 °C. Therefore, a uniform grain structure was obtained within 100 s annealing (Figs. 8e, 9e). In a study by Ravi Kumar and Sharma [54] in austenitic 304L stainless steel, it is suggested that the recrystallization process is continuous, as they identified sub-grains and recrystallized bands in the retained austenite grains generated during the repetitive annealing processes. Figures 8b, c and 9b, c show that simultaneous reversion of martensite and recrystallization of retained austenite resulted in a nonuniform grain size distribution at 700 °C. At 850 °C, the recrystallization is fast and a more uniform grain size distribution was achieved, although the grain size was not as small as at lower temperatures. At this temperature, grain coarsening also takes place but the grain size in the order of 0.45–1.01 μm was obtained in the C06–N27 steel.

One may notice that further grain refinement would need a higher cold reduction and faster recrystallization, both of which are demanding in practice. Reducing the austenite stability via adjusting its chemical composition would also be helpful for this purpose.

4.3 The Effect of Reversion Annealing on Mechanical Properties

In both steels, low-temperature annealing (i.e. 700 °C for 10 s) resulted in reverted, non-recrystallized microstructure

consisting of shear-reverted highly dislocated austenite and sub-boundaries, diffusion-reverted nano/ultrafine grained austenite, and large-grained cold deformed austenite (Figs. 8, 9). It is seen that yield strength is above 1090 MPa for these steels. Elongation of steels is lower than the fully annealed structures (36% in best condition) and SHR remains rather low. The yield strength is increased because of the slightly recovered cold-rolled austenitic microstructure with high dislocation density. Following an extended annealing of 1000 s at 700 °C, the microstructure contained new nano/ultrafine austenite grains and recovered, partially recrystallized retained austenite grains. Same as alloys with bimodal grain size distribution, the softer phase (*e.g.* retained austenite) is firstly deformed plastically under tension. It is already shown that the formation of α' -martensite is more readily in the coarse-grained austenite than the fine ones [45]. The grain size variation might justify the big difference between the observed mechanical properties and SHR behavior.

Uniform grain structure was formed in both steels after annealing at 850 °C for 100 s and above (Figs. 8, 9). The yield strength is smaller than the nonuniform grain structure, but still moderately bigger than that of the conventional steels because of the fine grain size (average grain size about 1 μm). In addition, one may notice that the yield strength of an order of 1100 MPa with a reasonable elongation is provided by reversion and partial recrystallization (at 700 °C), despite the nonuniform grain size.

The present work is in progress to determine kinetics of the austenite reversion and recrystallization and to develop processing map for the Ni-free ASSs containing different amounts of the C and N interstitial elements.

5 Conclusions

This study investigates the reversion annealing of the strain-induced α' -martensite in the 80% cold rolled metastable Ni-free ASSs containing 0.3 wt% (C + N). Significant grain refinement and strengthening was found by the application of the martensite reversion treatment. The main findings are listed below:

1. The martensite to austenite reversion process took place rapidly at 700 °C in both investigated steels. Both shear and diffusion types of the reversion process was detected at temperature 700 °C according to the features of fine and large austenite grains as well as low-angle grain boundaries. Recrystallization of the retained shear-reverted austenite at 700 °C took more than 1000 s.
2. A nonuniform microstructure is formed at 700 °C due to the fast formation of nano/ultrafine grains through reversion and of coarse grains by slow recrystallization of the retained austenite. The average austenite grain size was

evaluated to be approximately 0.32–1.02 μm depending on the annealing temperature.

3. Increasing annealing time and temperature resulted in more uniform microstructure due to the coarsening of the reverted ultrafine grains. A uniform austenite grain size of about 1 μm was acquired by reversion at 850 °C for 1000 s in both investigated steels.
4. The composite like structure consisting of the reverted austenite and the partially recrystallized austenite grains possessed significant synergy of enhanced strength and high uniform elongation.
5. The steel with higher C/N ratio showed lower strain hardening rates than the lower C/N ratio steel. It seems that addition of C to the Ni-free ASSs deteriorates mechanical properties by retardation of strain-induced martensite formation. Best results were obtained in the test material with lower C/N ratio.

Acknowledgements The financial support from the Iran National Science Foundation (Research Project No. 93045849) is gratefully acknowledged.

References

1. K.H. Lo, C.H. Shek, J.K.L. Lai, *Mater. Sci. Eng. R* **65**(4–6), 39–104 (2009)
2. M. Talha, C.K. Behera, O.P. Sinha, *Mater. Sci. Eng. C* **33**(7), 3563–3575 (2013)
3. J. Black, *Handbook of Biomaterials Properties* (Chapman & Hall, London, 1998)
4. K. Tomimura, S. Takaki, Y. Tokunaga, *ISIJ Int.* **31**(12), 1431–1437 (1991)
5. M.C. Somani, P. Juntunen, L.P. Karjalainen, R.D.K. Misra, A. Kyröläinen, *Metall. Mater. Trans. A* **40**(3), 729–744 (2009)
6. V.S.A. Challa, R.D.K. Misra, M.C. Somani, Z.D. Wang, *Mater. Sci. Eng. A* **649**, 153–157 (2016)
7. P. Behjati, A. Kermanpur, A. Najafizadeh, H.S. Baghbadorani, *Mater. Sci. Eng. A* **592**, 77–82 (2014)
8. M. Eskandari, A. Kermanpur, A. Najafizadeh, *Mater. Lett.* **63**(16), 1442–1444 (2009)
9. R.D.K. Misra, S. Nayak, P.K.C. Venkatasurya, V. Ramuni, M.C. Somani, L.P. Karjalainen, *Metall. Mater. Trans. A* **41**(8), 2162–2174 (2010)
10. S. Rajasekhara, L.P. Karjalainen, A. Kyröläinen, P.J. Ferreira, *Mater. Sci. Eng. A* **527**(7–8), 1986–1996 (2010)
11. S. Srikanth et al., *Int. J. Metall. Eng.* **2**(2), 203–213 (2013)
12. A. Di Schino, I. Salvatori, J.M. Kenny, *J. Mater. Sci.* **37**(21), 4561–4565 (2002)
13. F. Forouzan, A. Kermanpur, A. Najafizadeh, A. Hedayati, *Int. J. Mod. Phys. Conf. Ser.* **05**, 383–390 (2012)
14. M. Eskandari, A. Najafizadeh, A. Kermanpur, *Mater. Sci. Eng. A* **519**(1–2), 46–50 (2009)
15. M. Moallemi, A. Najafizadeh, A. Kermanpur, A. Rezaee, *Mater. Sci. Eng. A* **530**(1), 378–381 (2011)
16. H. Samaei Baghbadorani, A. Kermanpur, A. Najafizadeh, P. Behjati, A. Rezaee, M. Moallemi, *Mater. Sci. Eng. A* **636**, 593–599 (2015)

17. A. Rezaee, A. Kermanpur, A. Najafzadeh, M. Moallemi, *Mater. Sci. Eng. A* **528**(15), 5025–5029 (2011)
18. M. Sumita, T. Hanawa, S.H. Teoh, *Mater. Sci. Eng. C* **24**(6–8), 753–760 (2004)
19. R.P. Reed, *JOM* **41**(3), 16–21 (1989)
20. P.J. Uggowitzer, R. Magdowski, M.O. Speidel, *ISIJ Int.* **36**(7), 901–908 (1996)
21. M.O. Speidel, *Materwiss. Werksttech.* **37**(10), 875–880 (2006)
22. F.B. Pickering, *Int. Mater. Rev.* **21**, 42 (1976)
23. J. Rawers, M. Grujicic, *Mater. Sci. Eng. A* **207**(2), 188–194 (1996)
24. Z. Yuan, Q. Dai, X. Cheng, K. Chen, W. Xu, *Mater. Sci. Eng. A* **475**(1–2), 202–206 (2008)
25. G. Balachandran, M.L. Bhatia, N.B. Ballal, P.K. Rao, *ISIJ Int.* **41**(9), 1018–1027 (2001)
26. V.G. Gavriljuk, B.D. Shanina, H. Berns, *Mater. Sci. Eng. A* **481–482**(1–2 C), 707–712 (2008)
27. H. Berns, V.G. Gavriljuk, S. Riedner, A. Tyshchenko, *Steel Res. Int.* **78**(9), 714–719 (2007)
28. V.G. Gavriljuk, O.N. Razumov, Y.N. Petrov, I. Surzhenko, H. Berns, *Steel Res. Int.* **78**(9), 720–723 (2007)
29. B.D. Shanina, V.G. Gavriljuk, H. Berns, *Steel Res. Int.* **78**(9), 724–728 (2007)
30. T.-H. Lee, H.-Y. Ha, B. Hwang, S.-J. Kim, E. Shin, *Metall. Mater. Trans. A* **43**(12), 4455–4459 (2012)
31. H.-Y. Ha, T.-H. Lee, C.-S. Oh, S.-J. Kim, *Steel Res. Int.* **80**, 488–492 (2009)
32. J. Kang, F.C. Zhang, X.Y. Long, Z.N. Yang, *Mater. Sci. Eng. A* **610**, 427–435 (2014)
33. H. Feichtinger, G. Stein, *Mater. Sci. Forum* **318–320**, 261–270 (1999)
34. H. Berns, V. Gavriljuk, S. Riedner, *High Interstitial Stainless Austenitic Steels* (Springer, Berlin, 2013)
35. Y. Murata, O. Seiichi, U. Yoshihiro, *ISIJ Int.* **33**(7), 711–720 (1993)
36. Y. Hosoi, *J. Nucl. Mater.* **179–181**(part 1), 143–147 (1991)
37. Y. Hosoi, Y. Shimoide, M. Abraham, M. Kutsuna, K. Miyahara, *J. Nucl. Mater.* **191–194**, 686–690 (1992)
38. K. Miyahara, D.S. Bae, Y. Shimoide, *J. Nucl. Mater.* **212**, 766–771 (1994)
39. L. Mújica Roncery, S. Weber, W. Theisen, *Acta Mater.* **59**(16), 6275–6286 (2011)
40. V.G. Gavriljuk, *ISIJ Int.* **36**(7), 738–745 (1996)
41. Q.X. Dai, Z.Z. Yuan, X.M. Luo, X.N. Cheng, *Mater. Sci. Eng. A* **385**(1–2), 445–448 (2004)
42. J. Talonen, P. Nenonen, G. Pape, H. Hänninen, *Metall. Mater. Trans. A* **36**, 421–432 (2005)
43. ASTM E8-00, *Standard Method for Tension Testing of Metallic Materials* (West Conshohocken, West Conshohocken, 2001)
44. T. Masumura, N. Nakada, T. Tsuchiyama, S. Takaki, T. Koyano, K. Adachi, *Acta Mater.* **84**, 330–338 (2015)
45. Y. Matsuoka, T. Iwasaki, N. Nakada, T. Tsuchiyama, S. Takaki, *ISIJ Int.* **53**(7), 1224–1230 (2013)
46. D.P. Escobar, S.S. Ferreira de Dafé, D.B. Santos, *J. Mater. Res. Technol.* **4**(2), 162–170 (2015)
47. S. Sadeghpour, A. Kermanpur, A. Najafzadeh, *Mater. Sci. Eng. A* **584**, 177–183 (2013)
48. V.G. Gavriljuk, B.D. Shanina, H. Berns, *Acta Mater.* **48**(15), 3879–3893 (2000)
49. A. Kisko, R.D.K. Misra, J. Talonen, L.P. Karjalainen, *Mater. Sci. Eng. A* **578**, 408–416 (2013)
50. P. Behjati et al., *Mater. Des.* **63**, 500–507 (2014)
51. R.E. Schramm, R.P. Reed, *Metall. Trans. A* **6**(7), 1345–1351 (1975)
52. P.J. Brofman, G.S. Ansell, *Metall. Trans. A* **9A**, 879–880 (1978)
53. R.P. Reed, M.W. Austin, *Scr. Metall.* **23**, 1359–1362 (1989)
54. B. Ravi Kumar, S. Sharma, *Metall. Mater. Trans. A* **45**(13), 6027–6038 (2014)
55. L.F.M. Martins, R.L. Plaut, A.F. Padilha, F.M. Martins, R.L. Plaut, A.F. Padilha, *ISIJ Int.* **38**(6), 572–579 (1998)
56. L. Kaufman, E. Clougherty, R. Weiss, *Acta Metall.* **11**(5), 323–335 (1963)
57. Y. Lee, H. Shin, D. Leem, J. Choi, W. Jin, C. Choi, *Mater. Sci. Technol.* **19**, 393–399 (2003)
58. D. Leem, Y. Lee, J. Jun, *Scr. Mater.* **45**, 767–772 (2001)
59. A.F. Padilha, R.L. Plaut, P.R. Rios, *ISIJ Int.* **43**(2), 135–143 (2003)

Publisher's Note Springer Nature remains neutral with regard to jurisdictional claims in published maps and institutional affiliations.